

# Magnetic control of spin-orbit fields: a first-principles study of Fe/GaAs junctions

Martin Gmitra,<sup>1</sup> Alex Matos-Abiague,<sup>1</sup> Claudia Draxl,<sup>2</sup> and Jaroslav Fabian<sup>1</sup>

<sup>1</sup>*Institute for Theoretical Physics, University of Regensburg, 93040 Regensburg, Germany*

<sup>2</sup>*Physics Department, Humboldt-Universität zu Berlin, 12489 Berlin, Germany*

The microscopic structure of spin-orbit fields for the technologically important Fe/GaAs interface is uncovered from first principles. A symmetry based method allows to obtain the spin-orbit fields—both their magnitude and orientation—for a generic Bloch state, from the electronic band structure for any in-plane magnetization orientation. It is demonstrated that the spin-orbit fields depend not only on the electric field across the interface, but also surprisingly strongly on the Fe magnetization orientation, opening prospects for their magnetic control. These results give important clues in searching for spin-orbit transport and optical phenomena in ferromagnetic/nonmagnetic systems.

PACS numbers: 72.25.Mk, 73.20.-r, 75.76.+j

In solid-state systems lacking space inversion symmetry spin-orbit coupling (SOC) acts on the electronic structure as a spin-orbit field (SOF), which is an effective magnetic field whose direction and magnitude depend on the electron momentum [1, 2]. The most prominent examples are the Dresselhaus spin-orbit field [3] describing the effects of bulk inversion asymmetry (BIA) in zinc-blende semiconductors, and the Bychkov-Rashba spin-orbit field [4], describing the effects of structure inversion asymmetry (SIA) in asymmetric quantum wells. Apart from semiconductor structures, where Bychkov-Rashba coupling has been extensively studied [2, 5, 6] it has been investigated in many other systems, for example on metallic surfaces [7–12], graphene on a Ni substrate [13], or in Au and Ag monolayers on W(110) substrates [14]. A striking manifestation of spin-orbit coupling in condensed matter is the spin-momentum locking in topological insulators [15].

Spin-orbit coupling can be controlled by an electric field [16]. This fact has for long been used to motivate spintronics applications as epitomized by the Datta-Das transistor [17] in which the gate controls the spin-orbit induced spin precession of the itinerant electrons in a transistor channel. But spin-orbit coupling is also important for anisotropic magnetotransport. Tunneling anisotropic magnetoresistance (TAMR), for example, can be used to control electrical transport by rotating the magnetization orientation of a single ferromagnetic layer. It has been observed and studied in a variety of systems, GaMnAs/Al [18], Fe/GaAs, [2, 19], CoFe/GaAs [20] (inserting an MgO barrier suppresses TAMR here [21], a clear evidence for interface induced symmetry of the effect), Co/Pt [22], Si/ferromagnet junctions [23], resonant tunnel devices [24], or on an atomic scale in STM experiments [25]. Interfacial spin-orbit coupling has been proposed to control thermoelectric anisotropies in helimagnetic tunnel junctions [26] and produce spin-transfer torque in ferromagnet-topological insulator junctions [27].

In earlier studies of spin-orbit coupling on surfaces [7–9, 11, 12, 28] and interfaces [13, 14] the spin-orbit Hamil-

tonian was extracted by fitting the energy bands close to the  $\Gamma$  point assuming a Bychkov-Rashba-type coupling. This standard procedure requires *a priori* knowledge of the specific functional form of the spin-orbit field and applies only to very small  $\mathbf{k}$ -vectors for which small-momentum expansions are meaningful. Here we introduce a novel method to obtain spin-orbit fields (not just the functional parameters) for a generic  $\mathbf{k}$ -point directly from *ab-initio* data. On the example of an Fe/GaAs junction, important for room temperature spin injection [29–33] and TAMR [19, 34], we derive a formula for the magnitude and direction of the momentum dependent spin-orbit fields directly from the electronic band structure. The results show highly anisotropic (with respect to the momentum orientation) patterns, which take on different forms, from the ones known in semiconductor physics for small momenta to more exotic ones for Bloch states further away from the  $\Gamma$  point.

One fascinating outcome is a qualitative dependence of the spin-orbit fields patterns on the band (energy), consistent with the bias-induced inversion of the TAMR observed in experiments [19, 35]. Even more important, in addition to their sensitivity on an electric field, the spin-orbit fields can depend unusually strongly on the magnetization direction, to the point that the anisotropy axes can be flipped by rotating the magnetization. We emphasize that those effects are caused by the symmetry of the interface, not of the bulk structures, making them particularly important for lateral transport in ultrathin hybrid ferromagnet-nonmagnet junctions.

We consider thin Fe/GaAs slabs. The small lattice mismatch between Fe (2.87 Å) and GaAs (5.65 Å) allows for a smooth epitaxial growth of Fe on a GaAs (001) surface. Early investigations of the stability of  $1 \times 1$  Fe/GaAs interfaces within density functional theory [36] showed that when more than two atomic layers of Fe are deposited on a GaAs (001) surface, the flat or partially intermixed interfaces are more stable than the fully intermixed one, the As-terminated flat interface being more stable than the partially intermixed one. On the other hand, a recent Z-contrast scanning transmission electron

microscopy reported a single plane of alternating Fe and As atoms at an Fe/AlGaAs interface [37, 38]. Since the choice of the interface is not important to the message of our paper, we choose an As-terminated flat interface.

The electronic structure of an ideal Fe/GaAs slab, containing 9 (001) atomic layers of GaAs with the diagonal lattice spacing  $d = a/\sqrt{2} = 3.997 \text{ \AA}$  and three atomic planes of bcc Fe, has been calculated using the full potential linearized augmented plane wave technique implemented in the FLEUR code [39] and a generalized gradient approximation for the exchange-correlation functional [40]. The SOC has been treated within the second variational method.

The band structure of the Fe/GaAs slab along the high symmetry lines connecting the S –  $\Gamma$  – X points in the Brillouin zone (BZ) is shown in Fig. 1 for a magnetization orientation along the  $[1\bar{1}0]$  direction. The spin character of bands 1 and 2 in Fig. 1 is basically determined by the interface atoms. The interface unit cell contains interfacial As, the neighboring Ga, and two Fe atoms. The spin-up character of band  $n = 2$  is dominated by the interfacial As atom, its neighboring Ga atom and Fe atom above Ga, while the spin-down character of band  $n = 1$  comes mostly from the two Fe atoms.

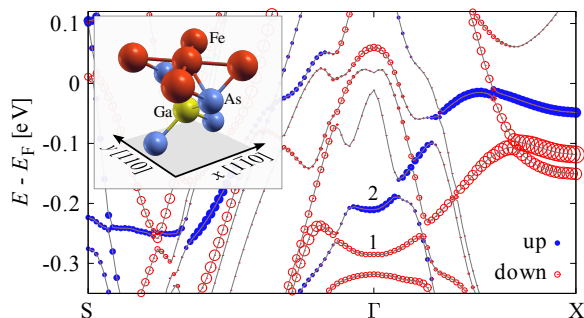


FIG. 1: Calculated band structure for the Fe/GaAs slab and magnetization along  $[1\bar{1}0]$ . The states with spin-up (spin-down) character at the Fe/GaAs interface are emphasized by blue filled (red open) circles whose radii are proportional to the corresponding charge density at the interface atoms. The inset shows the As-terminated flat  $1 \times 1$  interface model assumed in the study.

The non-centrosymmetric GaAs layer is of  $D_{2d}$  symmetry, exhibiting the BIA spin-orbit coupling. The interface lowers the symmetry to  $C_{2v}$  with the twofold rotation axis  $C_2$  along the growth direction  $[001]$  [2]. The  $C_{2v}$  symmetry accounts for both the BIA and SIA; the  $C_{2v}$  spin-orbit field lies in the plane of the slab, perpendicular to the growth direction. Since  $C_{2v}$  symmetry has only one-dimensional orbital irreducible representations, away from accidental level (anti)crossings the spin-orbit fields (even at high symmetry points) can be described by spin 1/2 Pauli matrices.

The most general SOC Hamiltonian consistent with  $C_{2v}$  symmetry can be written for the in-plane momenta

around the  $\Gamma$  point as

$$\mathcal{H}_{\text{so}} = \mu_n(k_x, k_y, \theta)k_x\sigma_y + \eta_n(k_x, k_y, \theta)k_y\sigma_x, \quad (1)$$

where  $k_x$  and  $k_y$  are the components of the in-plane wave vector  $\mathbf{k}$ ,  $\sigma_x$  and  $\sigma_y$  are the Pauli matrices, and  $x$  and  $y$  correspond to the diagonal  $[1\bar{1}0]$  and  $[110]$  crystallographic directions in GaAs, respectively;  $\theta$  refers to the magnetization direction with respect to the  $[1\bar{1}0]$  crystallographic direction of GaAs and  $n$  labels the band of interest. The functional parameters  $\mu_n$  and  $\eta_n$ ,

$$\begin{aligned} \mu_n(k_x, k_y, \theta) &= \mu_n^{(0)}(\theta) + \mu_n^{(1)}(\theta)k_x^2 + \mu_n^{(2)}(\theta)k_y^2 + \dots, \\ \eta_n(k_x, k_y, \theta) &= \eta_n^{(0)}(\theta) + \eta_n^{(1)}(\theta)k_x^2 + \eta_n^{(2)}(\theta)k_y^2 + \dots \end{aligned} \quad (2)$$

are even in the momenta and, what is crucial and new here, depend in general on the magnetization direction.

The values of the expansion parameters  $\mu_n^{(i)}, \eta_n^{(i)}$  ( $i = 0, 1, 2, \dots$ ) determine the specific form of the SOF. For example, if  $\mu_n^{(0)} = \alpha_n$  and  $\eta_n^{(0)} = -\alpha_n$  ( $\mu_n^{(0)} = \eta_n^{(0)} = \beta_n$ ),  $\mathcal{H}_{\text{so}}$  reduces in the limit of small  $k = |\mathbf{k}|$  to the well known Bychkov-Rashba [4] (linearized Dresselhaus [3]) SOC with  $\alpha_n$  ( $\beta_n$ ) denoting the Bychkov-Rashba (Dresselhaus) SOC parameter of the  $n$ th band. By introducing the SOF field

$$\mathbf{w}_n(k_x, k_y, \theta) = \begin{pmatrix} \eta_n(k_x, k_y, \theta)k_y \\ \mu_n(k_x, k_y, \theta)k_x \\ 0 \end{pmatrix}, \quad (3)$$

Eq. (1) can be rewritten as  $\mathcal{H}_{\text{so}} = \mathbf{w}_n(\mathbf{k}) \cdot \boldsymbol{\sigma}$ , where  $\boldsymbol{\sigma}$  is the vector of the Pauli matrices.

We first analyze the spin-orbit fields for in-plane magnetization directions. Since the exchange field dominates over spin-orbit coupling and the magnetization lies in the plane of the layers, the SOC contribution to the energy can be treated within first order perturbation theory. From the symmetry properties we find (see the Supplementary Material for the details) the following relations,

$$w_{nx}(\mathbf{k}, \theta) = \sigma \left[ \frac{\Delta E_n^{\text{so}}(\mathbf{k}, \theta) + \Gamma_n^{\text{so}}(\mathbf{k}, \theta)}{2 \cos \theta} \right] \quad (4)$$

and

$$w_{ny}(\mathbf{k}, \theta) = \sigma \left[ \frac{\Delta E_n^{\text{so}}(\mathbf{k}, \theta) - \Gamma_n^{\text{so}}(\mathbf{k}, \theta)}{2 \sin \theta} \right] \quad (5)$$

where

$$\Delta E_n^{\text{so}}(\mathbf{k}, \theta) = \frac{E_n(\mathbf{k}, \theta) - E_n(-\mathbf{k}, \theta)}{2}, \quad (6)$$

$$\Gamma_n^{\text{so}}(\mathbf{k}, \theta) = \frac{E_n(-k_x, k_y, \theta) - E_n(k_x, -k_y, \theta)}{2}, \quad (7)$$

and  $\sigma$  refers to the spin character of the  $n$ th band. The above relations allow us to extract the components of

the SOF directly from the *ab-initio* energy bands. In the particular cases of  $\theta \approx \pi/2$  and  $\theta \approx 0$  the numerators and denominators in Eqs. (4) and (5), respectively, vanish. In such cases the SOF is obtained by L'Hôpital's rule. The validity of Eqs. (4) and (5) is not restricted to the vicinity of the  $\Gamma$  point but holds also for large momenta. The only restriction is that the  $k$ -space region of interest must be away from energy anticrossings.

Figure 2 establishes the proof of principle for the magnetization dependence of SOFs. It shows the SOF,  $\mathbf{w}(\mathbf{k})$  (bottom parts), and polar plots of its strength  $w = |\mathbf{w}(\mathbf{k})|$  (upper parts), for the interface band  $n = 1$ . The SOF is computed on three different contours around the  $\Gamma$  point,  $k = \pi/100d$ ,  $\pi/8d$  and  $\pi/5d$  and plotted in Figs. 2a), b), and c), respectively. The left (right) panel corresponds to the magnetization pointing along  $[1\bar{1}0]$  ( $[110]$ ). The  $C_{2v}$  symmetry of the SOF is preserved for all  $k$ . In particular, close to the  $\Gamma$  point the SOFs resemble the interference of Bychkov-Rashba-type and Dresselhaus-type SOC (see Fig. 2a). However, away from the  $\Gamma$  point higher in  $k$  terms become relevant and more exotic patterns—we call them spin-orbit-field butterflies—in the SOF appear (see Fig. 2b, c). The linear terms are dominant up to about 5% from the BZ center, where the SOF exhibits a very strong dependence on the magnetization orientation. Note that the principal symmetry axes of the SOF can even be flipped by turning the magnetization orientation. This remarkable effect opens the perspective of a magnetic control of spin-orbit fields.

Close to the  $\Gamma$  point the SOF is determined by the contributions linear in the wave vector components  $k_x$  and  $k_y$  and characterized by Bychkov-Rashba-type and Dresselhaus-type SOC parameters,  $\alpha_n = [\mu_n^{(0)} - \eta_n^{(0)}]/2$  and  $\beta_n = [\mu_n^{(0)} + \eta_n^{(0)}]/2$ , respectively. Using Eqs. (2)-(6) we obtain, (see Supplementary Material for more details),

$$\alpha_n(\theta) = \sigma \left[ \frac{a_n(\theta) \cos \theta - b_n(\theta) \sin \theta}{\sin(2\theta)} \right], \quad (8)$$

and

$$\beta_n(\theta) = \sigma \left[ \frac{a_n(\theta) \cos \theta + b_n(\theta) \sin \theta}{\sin(2\theta)} \right], \quad (9)$$

where  $a_n(\theta) = \partial E_n(\mathbf{k}, \theta) / \partial k_x|_{k=0}$  and  $b_n(\theta) = \partial E_n(\mathbf{k}, \theta) / \partial k_y|_{k=0}$ . Thus, the dependence of  $\alpha_n(\theta)$  and  $\beta_n(\theta)$  on the magnetization orientation can be obtained by computing the  $k$ -space gradient (velocity) of the *ab-initio* energy bands in the vicinity of the  $\Gamma$  point. The functional forms of  $a_n(\theta)$  and  $b_n(\theta)$  conform to the symmetry requirements (see Supplementary Material).

Figure 3 shows the magnetization dependence of the Bychkov-Rashba-type and Dresselhaus-type SOC parameters for the interface bands. The SOC parameters exhibit an oscillatory behavior as a function of the magnetization orientation. The angular dependence of the SOC

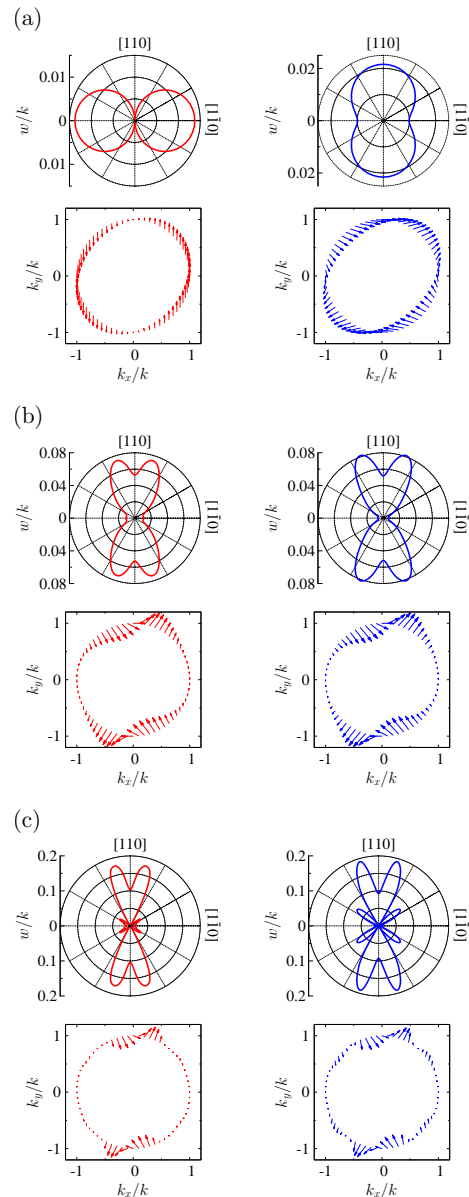


FIG. 2: Spin-orbit-field “butterflies”. Calculated spin-orbit fields for the magnetization along  $[1\bar{1}0]$  (left) and  $[110]$  (right). The polar plots of the spin-orbit coupling strength ( $w/k$ ) in the units of  $\text{eV \AA}$  as well as the corresponding vector fields  $\mathbf{w}(\mathbf{k})$  are shown for the band  $n = 1$  and the momentum contours of (a)  $k = \pi/100d$ ; (b)  $k = \pi/8d$ ; (c)  $k = \pi/5d$ . The lengths of the direction vectors have been rescaled.

parameters is stronger for band  $n = 1$  than for  $n = 2$ . In particular, for the case of band  $n = 1$  the Bychkov-Rashba-type SOC parameter can even change its sign when the magnetization is rotated in the plane. This leads to the sign change of the product  $\alpha_1\beta_1$  when the magnetization is rotated from  $[1\bar{1}0]$  to  $[110]$  and produces the flipping of the SOF symmetry axes shown in Fig. 2a). For band  $n = 2$  the angular dependence is weaker, the product  $\alpha_2\beta_2$  does not change its sign and the symmetry

axis of the SOF is preserved, being independent of the magnetization orientation.

When considering the dependence on the transverse electric field, the behavior is opposite. Indeed, while the SOC parameters corresponding to band  $n = 1$  change very little with  $E$ , for band  $n = 2$  the changes in the magnitudes of  $\alpha_2$  and  $\beta_2$  are appreciable. This disparate behavior is a consequence of the different nature of these two bands. Band  $n = 1$  originates mostly from the two Fe atoms in the interface unit cell and, therefore, its corresponding SOF is more sensible to the changes in the magnetization direction. However, the electrostatic control of the SOC parameters is dominated by the electric field influence on the  $pd$  bonding between As and Fe atoms. Consequently, the SOF corresponding to band  $n = 2$ , which comes mostly from the interfacial As atom, its neighboring Ga and the Fe atom above Ga, exhibits a stronger dependence on the electric field.

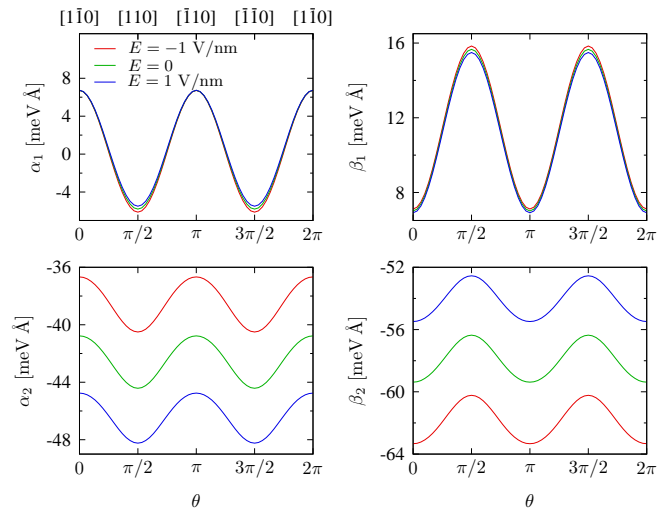


FIG. 3: Calculated magnetization and electric field dependence of the spin-orbit coupling parameters. The Bychkov-Rashba-type  $\alpha_n$  and the Dresselhaus-type  $\beta_n$  spin-orbit parameters for the interface bands  $n = 1, 2$  are shown as a function of the in-plane magnetization orientation and for different electric fields.

In Table I we list the expansion coefficients of the SOC parameters [see Eqs. (23-24) in the Supplementary Material],

$$\alpha_n \simeq A_n^{(+)} + B_n^{(+)} \cos(2\theta), \quad (10)$$

$$\beta_n \simeq A_n^{(-)} + B_n^{(-)} \cos(2\theta), \quad (11)$$

for zero electric field. From  $A_n^{(+/-)}$  one extracts the magnetization-independent part, whereas the  $B_n^{(+/-)}$  parameters control the leading contribution (higher order coefficients are about two orders smaller) to the angular (magnetization orientation) dependence of the spin-orbit parameters. In addition to the interface bands ( $n = 1, 2$ ) we have also included the expansion coefficients corre-

sponding to the As-surface bands ( $n = 3, 4$ ), which due to their surface nature possess stronger SOFs.

$n$	$A_n^{(+)}$	$B_n^{(+)}$	$A_n^{(-)}$	$B_n^{(-)}$
1	-0.42	-6.26	-11.32	4.32
2	-42.51	1.82	-57.94	-1.51
3	-620.24	-88.74	-597.56	-89.62
4	680.09	95.61	697.58	103.15

TABLE I: Band-resolved expansion coefficients of the Bychkov-Rashba-type and Dresselhaus-type spin-orbit coupling parameters in meV Å units. The parameters are in the range of what is found in semiconductors [2]),

If the magnetization is perpendicular to the interface plane, the first order correction to the energy vanishes and the methodology used for the case of in-plane magnetization does not apply. To extract useful information about SOFs we first note that the in-plane components of the spin appear due to SOFs only (without spin-orbit coupling the electron spins would be fully polarized in the growth direction). Since the exchange field dominates over SOC, the spin is still quantized largely along the magnetization direction, so the expectation values of the transverse components of the spin  $\langle \mathbf{s} \rangle_n$  corresponding to the  $n$ th band can be obtained by considering  $\mathcal{H}_{\text{SO}}$  as a perturbation. First order perturbation theory gives

$$\langle s_x \rangle_n = w_{nx} / \Delta_{\text{xc}} \quad ; \quad \langle s_y \rangle_n = w_{ny} / \Delta_{\text{xc}}, \quad (12)$$

where  $\Delta_{\text{xc}}$  is the exchange splitting energy and  $\hbar = 1$ . Using these approximate relations, we can determine the pattern of  $\mathbf{w}$ , but not its magnitude. Figure 4 shows  $\mathbf{w}(\mathbf{k})$  (right parts), and its rescaled magnitude  $w = |\mathbf{w}(\mathbf{k})|$  (left parts) in the units of the exchange splitting  $\Delta_{\text{xc}}$  for the interface band  $n = 1$ . The fields have been computed on two contours,  $k = \pi/25d$  (a) and  $k = \pi/8d$  (b). Similar to the in-plane magnetization case, when the magnetization is perpendicular to the layers, the SOF close to the  $\Gamma$  point resembles the interference of the Bychkov-Rashba-type and Dresselhaus-type SOCs. The effect of a transverse electric field quantitatively modifies the SOF and is more pronounced for larger  $k$  values [see Fig. 4b)].

To summarize, we introduced a method to calculate spin-orbit fields from first principles and applied it to the Fe/GaAs interface. We found the the spin-orbit fields depend strongly on the Fe magnetization direction. This finding should be particularly important for lateral and tunneling magnetotransport anisotropies of ferromagnet-nonmagnet slabs.

We thank D. Weiss, G. Bayreuther, C. Back, G. Woltersdorf for useful hints related to experimental ramifications of the presented theoretical concepts and F. Freimuth, Y. Mokrousov, G. Bihlmayer, J. Spitaler and P. Novák for helpful discussions regarding the calculations. This work has been supported by DFG SFB 689.

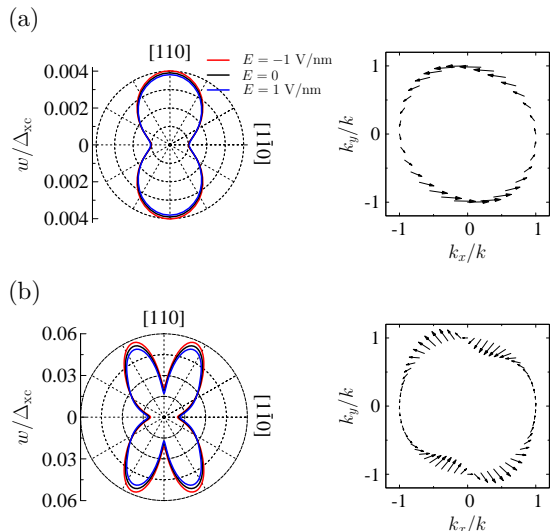


FIG. 4: Electric field control of the spin-orbit coupling for magnetization perpendicular to the plane. Polar plots of the spin-orbit field strength (left panel) corresponding to the interface band  $n = 1$  on the contours (a)  $k = \pi/25d$  and (b)  $k = \pi/8d$ , for transverse electric fields -1, 0, 1 V/nm. The momentum-dependent expectation values of the in-plane spin vectors  $\langle \mathbf{s} \rangle$  on the two corresponding  $k$ -contours is shown in the right panel for zero electric field. The size of the vectors has been rescaled.

[1] I. Žutić, J. Fabian, and S. Das Sarma, *Rev. Mod. Phys.* **76**, 323 (2004).  
 [2] J. Fabian, A. Matos-Abiague, C. Ertler, P. Stano, and I. Žutić, *Acta Phys. Slov.* **57**, 565 (2007).  
 [3] G. Dresselhaus, *Phys. Rev.* **100**, 580 (1955).  
 [4] Y. A. Bychkov and E. I. Rashba, *JETP Lett.* **39**, 78 (1984).  
 [5] R. Winkler, *Spin-orbit coupling effects in two-dimensional electron and hole systems* (Springer, Berlin, 2003).  
 [6] X. Cartoixá, L. W. Wang, D. Z. Y. Ting, and Y. C. Chang, *Phys. Rev. B* **73**, 205341 (2006).  
 [7] S. LaShell, B. A. McDougall, and E. Jensen, *Phys. Rev. Lett.* **77**, 3419 (1996).  
 [8] J. Henk, A. Ernst, and P. Bruno, *Phys. Rev. B* **68**, 165416 (2003).  
 [9] Y. M. Koroteev, G. Bihlmayer, J. E. Gayone, E. V. Chulkov, S. Blügel, P. M. Echenique, and P. Hofmann, *Phys. Rev. Lett.* **93**, 046403 (2004).  
 [10] B. Fluegel, S. Francoeur, A. Mascarenhas, S. Tixier, E. C. Young, and T. Tiedje, *Phys. Rev. Lett.* **97**, 067205 (2006).  
 [11] C. R. Ast, J. Henk, A. Ernst, L. Moreschini, M. C. Falub, D. Pacilé, P. Bruno, K. Kern, and M. Grioni, *Phys. Rev. Lett.* **98**, 186807 (2007).  
 [12] F. Meier, H. Dil, J. Lobo-Checa, L. Patthey, and J. Osterwalder, *Phys. Rev. B* **77**, 165431 (2008).  
 [13] Y. S. Dedkov, M. Fonin, U. Rüdiger, and C. Laubschat, *Phys. Rev. Lett.* **100**, 107602 (2008).

[14] A. M. Shikin, A. Varykhalov, G. V. Prudnikova, D. Usachev, V. K. Adamchuk, Y. Yamada, J. Riley, and O. Rader, *Phys. Rev. Lett.* **100**, 057601 (2008).  
 [15] M. Z. Hasan and C. L. Kane, *Rev. Mod. Phys.* **82**, 3045 (2010).  
 [16] J. Nitta, T. Akazaki, H. Takayanagi, and T. Enoki, *Phys. Rev. Lett.* **78**, 1335 (1997).  
 [17] S. Datta and B. Das, *Appl. Phys. Lett.* **56**, 665 (1990).  
 [18] C. Gould, C. Rüster, T. Jungwirth, E. Girgis, G. M. Schott, R. Giraud, K. Brunner, G. Schmidt, and L. W. Molenkamp, *Phys. Rev. Lett.* **93**, 117203 (2004).  
 [19] J. Moser, A. Matos-Abiague, D. Schuh, W. Wegscheider, J. Fabian, and D. Weiss, *Phys. Rev. Lett.* **99**, 056601 (2007).  
 [20] T. Uemura, M. Harada, K. Matsuda, and M. Yamamoto, *Appl. Phys. Lett.* **96**, 252106 (2010).  
 [21] T. Akiho, T. Uemura, M. Harada, K. Matsuda, and M. Yamamoto, *Appl. Phys. Lett.* **98**, 232109 (2011).  
 [22] B. G. Park, J. Wunderlich, D. A. Williams, S. J. Joo, K. Y. Jung, K. H. Shin, K. Olejnik, A. B. Shick, and T. Jungwirth, *Phys. Rev. Lett.* **100**, 087204 (2008).  
 [23] S. Sharma, S. P. Dash, H. Saito, S. Yuasa, B. J. van Wees, and R. Jansen, *Phys. Rev. B* **86**, 165308 (2012).  
 [24] M. Tran, J. Peiro, H. Jaffres, J.-M. George, O. Manguin, L. Largeau, and A. Lemaitre, *Appl. Phys. Lett.* **95**, 172101 (2009).  
 [25] K. von Bergmann, M. Menzel, D. Serrate, Y. Yoshida, S. Schröder, P. Ferriani, A. Kubetzka, R. Wiesendanger, and S. Heinze, *Phys. Rev. B* **86**, 134422 (2012).  
 [26] C. Jia and J. Berakdar, *Appl. Phys. Lett.* **98**, 192111 (2011).  
 [27] F. Mahfouzi, N. Nagaosa, and B. K. Nikolic, *Phys. Rev. Lett.* **109**, 166602 (2012).  
 [28] O. Krupin, G. Bihlmayer, K. Starke, S. Gorovikov, J. E. Prieto, K. Döbrich, S. Blügel, and G. Kaindl, *Phys. Rev. B* **71**, 201403 (2005).  
 [29] A. T. Hanbicki, B. T. Jonker, G. Itskos, G. Kiöseoglou, and A. Petrou, *Appl. Phys. Lett.* **80**, 1240 (2002).  
 [30] S. A. Crooker, M. Furis, X. Lou, C. Adelman, D. L. Smith, C. J. Palmström, and P. A. Crowell, *Science* **309**, 2191 (2005).  
 [31] P. Kotissek, M. Bailleul, M. Sperl, A. Spitzer, D. Schuh, W. Wegscheider, C. H. Back, and G. Bayreuther, *Nature Phys.* **3**, 872 (2007).  
 [32] P. Mavropoulos, O. Wunnicke, and P. H. Dederichs, *Phys. Rev. B* **66**, 024416 (2002).  
 [33] A. Perlov, V. Popescu, and H. Ebert, *phys. stat. sol (b)* **241**, 1316 (2004).  
 [34] R. Sykora and I. Turek, *J. Phys. Cond. Matter* **24**, 365801 (2012).  
 [35] A. Matos-Abiague and J. Fabian, *Phys. Rev. B* **79**, 155303 (2009).  
 [36] S. C. Erwin, S. H. Lee, and M. Scheffler, *Phys. Rev. B* **65**, 205422 (2002).  
 [37] T. J. Zega, A. T. Hanbicki, S. C. Erwin, I. Žutić, G. Kiöseoglou, C. H. Li, B. T. Jonker, and R. M. Stroud, *Phys. Rev. Lett.* **96**, 196101 (2006).  
 [38] L. R. Fleet, H. Kobayashi, Y. Ohno, J. Y. Kim, C. H. W. Barnes, and A. Hirohata, *J. Appl. Phys.* **109**, 07C504 (2011).  
 [39] “See <http://www.flapw.de/>,” .  
 [40] J. P. Perdew, K. Burke, and M. Ernzerhof, *Phys. Rev. Lett.* **77**, 3865 (1996).

## SUPPLEMENTAL MATERIAL

### Magnetic control of spin-orbit fields: a first-principles study of Fe/GaAs junctions

Martin Gmitra,<sup>1</sup> Alex Matos-Abiague,<sup>1</sup> Claudia Draxl,<sup>2</sup> and Jaroslav Fabian<sup>1</sup>

<sup>1</sup>*Institute for Theoretical Physics, University of Regensburg, 93040 Regensburg, Germany*

<sup>2</sup>*Physics Department, Humboldt-Universität zu Berlin, 12489 Berlin, Germany*

#### I. GENERAL THEORY.

We describe our symmetry-based method to obtain the in-plane spin-orbit fields (SOF) from first-principles data.

In the presence of spin-orbit coupling (SOC) the energy bands become anisotropic with respect to the magnetization orientation  $\mathbf{m} = (\cos \theta, \sin \theta, 0)$ . The dispersion relation of the  $n$ th energy band can, in general, be written as

$$E_n(\mathbf{k}, \theta) = T_n(\mathbf{k}, \theta) + \Delta_n(\theta) + \Delta E_n^{\text{so}}(\mathbf{k}, \theta), \quad (1)$$

where  $T_n(\mathbf{k}, \theta)$  is even in  $\mathbf{k}$ . The  $\mathbf{k}$ -independent term  $\Delta_n(\theta)$  describes the overall energy shift at the  $\Gamma$  point and is related to both the exchange energy splitting and the intrinsic atomic SOC. The SOC induced by lack of inversion symmetry generates the contribution  $\Delta E_n^{\text{so}}(\mathbf{k}, \theta)$ , which is odd in  $\mathbf{k}$ . By time reversal symmetry, the energy bands must remain invariant under the simultaneous inversion of the wave vector and the magnetization direction, i. e.,  $E_n(\mathbf{k}, \theta) = E_n(-\mathbf{k}, \theta + \pi)$ . This, together with Eq. (1), allows for expressing the SOC correction in terms of the band energy,

$$\Delta E_n^{\text{so}}(\mathbf{k}, \theta) = \frac{E_n(\mathbf{k}, \theta) - E_n(-\mathbf{k}, \theta)}{2}. \quad (2)$$

In our system not only the interface confinement but also the magnetism reduce the symmetry and lift the band degeneracies at the  $\Gamma$  point, as shown in Fig. 1 of the article.<sup>4</sup> This allows for a description of the SOC in terms of Pauli matrices. As discussed in the article, the most general SOC Hamiltonian that exhibits  $C_{2v}$  symmetry can be written as,

$$\mathcal{H}_{\text{so}} = \mathbf{w}_n(\mathbf{k}, \theta) \cdot \boldsymbol{\sigma}, \quad (3)$$

where  $\boldsymbol{\sigma}$  are Pauli matrices and  $\mathbf{w}_n(\mathbf{k}, \theta)$ , whose components are

$$w_{nx}(\mathbf{k}, \theta) = \eta_n(k_x, k_y, \theta)k_y \quad ; \quad w_{ny}(\mathbf{k}, \theta) = \mu_n(k_x, k_y, \theta)k_x, \quad (4)$$

is the spin-orbit field (SOF) vector. The  $x$  and  $y$  axes refer to the principal symmetry axes of the  $C_{2v}$  symmetry. In our case  $x = [\bar{1}\bar{1}0]$  and  $y = [110]$ .

The most general functional form of  $\eta_n(k_x, k_y, \theta)$  and  $\mu_n(k_x, k_y, \theta)$  which is compatible with the  $C_{2v}$  symmetry of the SOF is given in Eq. (2) of the article. The functions  $\eta_n(k_x, k_y, \theta)$  and  $\mu_n(k_x, k_y, \theta)$  are even in both  $k_x$  and  $k_y$ . Therefore, the SOF components must obey the symmetry relations,

$$w_{nx}(k_x, k_y, \theta) = w_{nx}(-k_x, k_y, \theta) \quad ; \quad w_{ny}(k_x, k_y, \theta) = -w_{ny}(-k_x, k_y, \theta). \quad (5)$$

Since the exchange field dominates over SOC, the contribution of  $\mathcal{H}_{\text{so}}$  to the energy can be treated within first order perturbation theory, which yields the energy correction

$$\Delta E_n^{\text{so}}(\mathbf{k}, \theta) = \sigma [w_{nx}(\mathbf{k}, \theta) \cos \theta + w_{ny}(\mathbf{k}, \theta) \sin \theta], \quad (6)$$

where  $\sigma$  indicates whether the spin of the unperturbed band (i. e., in the absence of SOC) is parallel ( $\sigma = 1$ ) or antiparallel ( $\sigma = -1$ ) to the magnetization. Away from band anticrossings the effect of SOC on the spin orientation is small and does not change the spin character of the band. Therefore, away from anticrossings, we still can reliably identify  $\sigma = 1$  ( $\sigma = -1$ ) with the spin-up (spin-down) character of the perturbed energy band (i. e., in the presence of SOC).

Equation (2) together with Eq. (6) connect the SOF with the band energies. However, in order to extract  $w_{nx}(\mathbf{k}, \theta)$  and  $w_{ny}(\mathbf{k}, \theta)$  separately, additional symmetry constraints are needed. The Fe/GaAs interface exhibits a structural  $C_{2v}$  symmetry with the reflection planes  $(\bar{1}\bar{1}0)$  and  $(110)$  and  $[001]$  as the two-fold rotation axis (see Fig. 1). But when the magnetism of Fe is included, the symmetry is reduced and the  $C_{2v}$  symmetry of the energy contours

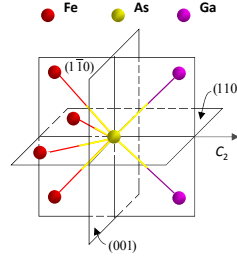


FIG. 1. Schematic of the atomic structure of an As-terminated Fe/GaAs interface. The symmetry of the interface is that of the point group  $C_{2v}$ , containing the twofold rotation axis  $C_2$  parallel to the growth direction  $[001]$  and the two mirror planes  $(1\bar{1}0)$  and  $(110)$ .

in the momentum space is destroyed. Nevertheless, additional symmetry constraints on  $w_{nx}(\mathbf{k}, \theta)$  and  $w_{ny}(\mathbf{k}, \theta)$  are found by considering the magnetization as a symmetry variable. Note, for example, that (we consider only  $0 \leq \theta < \pi/2$ ) the spatial reflection with respect to the plane  $(1\bar{1}0)$  is equivalent to the rotation of the magnetization by  $-2\theta$  around the  $[001]$  axis (see Fig. 2).<sup>5</sup> This implies that the energy contours in  $\mathbf{k}$ -space must fulfill the relation  $E_n(-k_x, k_y, \theta) = E_n(k_x, k_y, -\theta)$ , which according to Eqs. (1), (2), and (6) yields,

$$w_{nx}(k_x, k_y, -\theta) = w_{nx}(-k_x, k_y, \theta) \quad ; \quad w_{ny}(k_x, k_y, -\theta) = -w_{ny}(-k_x, k_y, \theta). \quad (7)$$

By combining Eqs. (5) and (7) we obtain the following symmetry constraints on the SOF components,

$$w_{nx}(k_x, k_y, \theta) = w_{nx}(k_x, k_y, -\theta) \quad ; \quad w_{ny}(k_x, k_y, \theta) = w_{ny}(k_x, k_y, -\theta), \quad (8)$$

which together with Eq. (6) leads to

$$w_{nx}(\mathbf{k}, \theta) = \sigma \left[ \frac{\Delta E_n^{\text{so}}(\mathbf{k}, \theta) + \Delta E_n^{\text{so}}(\mathbf{k}, -\theta)}{2 \cos \theta} \right] \quad ; \quad w_{ny}(\mathbf{k}, \theta) = \sigma \left[ \frac{\Delta E_n^{\text{so}}(\mathbf{k}, \theta) - \Delta E_n^{\text{so}}(\mathbf{k}, -\theta)}{2 \sin \theta} \right]. \quad (9)$$

With the help of Eq. (2) we can rewrite the above relations as,

$$w_{nx}(k_x, k_y, \theta) = \sigma \left[ \frac{E_n(\mathbf{k}, \theta) - E_n(-\mathbf{k}, \theta) + E_n(-k_x, k_y, \theta) - E_n(k_x, -k_y, \theta)}{4 \cos \theta} \right] \quad (10)$$

and

$$w_{ny}(k_x, k_y, \theta) = \sigma \left[ \frac{E_n(\mathbf{k}, \theta) - E_n(-\mathbf{k}, \theta) - E_n(-k_x, k_y, \theta) + E_n(k_x, -k_y, \theta)}{4 \sin \theta} \right], \quad (11)$$

which allows us to extract the SOF directly from *ab-initio* data.<sup>6</sup>

In the particular cases  $\theta = \pi/2$  and  $\theta = 0$  the numerators and denominators in Eqs. (10) and (11) vanish and the SOF can be obtained from L'Hôpital's rule.

## II. LINEAR SPIN-ORBIT FIELDS.

In the vicinity of the  $\Gamma$  point the SOF is linear in the wave vector components  $k_x$  and  $k_y$ . According to Eqs. (2) and (3) of the article, the linear contributions to the SOF are given by

$$w_{nx}^{(0)}(\mathbf{k}, \theta) = \eta_n^{(0)}(\theta) k_y \quad ; \quad w_{ny}^{(0)}(\mathbf{k}, \theta) = \mu_n^{(0)}(\theta) k_x, \quad (12)$$

where

$$\eta_n^{(0)}(\theta) = \left. \frac{\partial w_{nx}(\mathbf{k}, \theta)}{\partial k_y} \right|_{k=0} \quad ; \quad \mu_n^{(0)}(\theta) = \left. \frac{\partial w_{ny}(\mathbf{k}, \theta)}{\partial k_x} \right|_{k=0}. \quad (13)$$

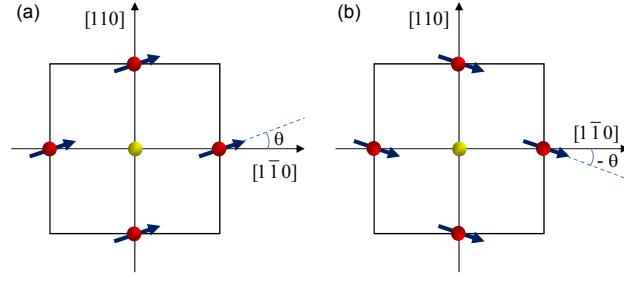


FIG. 2. (a) Top view of the investigated Fe/GaAs interface as seen from the interface plane of As atoms. The red spheres represent four Fe atoms nearest to the As atom (yellow sphere). The arrows represent the Fe magnetic moments aligned along the magnetization direction  $\mathbf{m} = (\cos \theta, \sin \theta, 0)$ . (b) The structure of (a) after a reflection with respect to the mirror plane  $(\bar{1}\bar{1}0)$  (recall that spins and magnetic moments are axial vectors). Alternatively, one can also obtain (b) from (a) by a rotation of the magnetization by the angle  $-2\theta$  around the  $[001]$  axis. This leads to the symmetry relation  $E_n(-k_x, k_y, \theta) = E_n(k_x, k_y, -\theta)$ .

Taking into account Eqs. (10) and (11) we obtain,

$$\eta_n^{(0)}(\theta) = \sigma \frac{b_n(\theta)}{\cos \theta} ; \quad \mu_n^{(0)}(\theta) = \sigma \frac{a_n(\theta)}{\sin \theta}, \quad (14)$$

where

$$a_n(\theta) = \left. \frac{\partial E_n(\mathbf{k}, \theta)}{\partial k_x} \right|_{k=0} ; \quad b_n(\theta) = \left. \frac{\partial E_n(\mathbf{k}, \theta)}{\partial k_y} \right|_{k=0}. \quad (15)$$

Thus, the size of the linear SOC induced by inversion asymmetry can be estimated by computing the  $\mathbf{k}$ -space gradient (velocity) of the *ab initio* energy bands in the vicinity of the  $\Gamma$  point.

The general form of coefficients  $a_n(\theta)$  and  $b_n(\theta)$  can be deduced from symmetry considerations. By time reversal symmetry,  $E_n(\mathbf{k}, \theta) = E_n(-\mathbf{k}, \theta + \pi)$  and, therefore, the following relations

$$a_n(\theta) = -a_n(\theta + \pi) ; \quad b_n(\theta) = -b_n(\theta + \pi) \quad (16)$$

must hold. On the other hand the constraint in Eq. (8) leads to

$$a_n(\theta) = -a_n(-\theta) ; \quad b_n(\theta) = b_n(-\theta). \quad (17)$$

Furthermore, since both  $a_n(\theta)$  and  $b_n(\theta)$  are periodic functions of  $\theta$ , they can be expanded in Fourier series. Thus, under the symmetry constrains in Eqs. (16) and (17) the corresponding Fourier expansions for  $a_n(\theta)$  and  $b_n(\theta)$  reduce to

$$a_n(\theta) = \sum_{l=0}^{\infty} a_{nl} \sin[(2l+1)\theta] \quad (18)$$

and

$$b_n(\theta) = \sum_{l=0}^{\infty} b_{nl} \cos[(2l+1)\theta], \quad (19)$$

respectively. For the bands investigated in the article we have found that for accurately fitting the band energy gradient at the  $\Gamma$  point it is enough to consider the first three terms in the series expansions of  $a_n$  and  $b_n$ . Thus, one can further approximate Eqs. (18) and (19) as

$$a_n(\theta) = a_{n0} \sin \theta + a_{n1} \sin(3\theta) + a_{n2} \sin(5\theta) \quad (20)$$

and

$$b_n(\theta) = b_{n0} \cos \theta + b_{n1} \cos(3\theta) + b_{n2} \cos(5\theta), \quad (21)$$

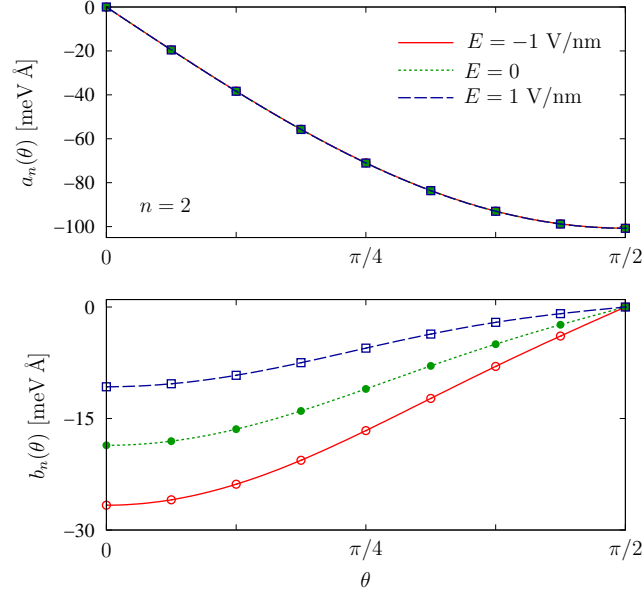


FIG. 3. Calculated spin-orbit coupling coefficients ( $a_n$  and  $b_n$ ) for the Fe/GaAs slab corresponding to the interface band  $n = 2$  as a function of the magnetization orientation. The lines are fittings of Eqs. (20) and (21) to the *ab-initio* data (dots). The data are obtained by using Eq. (15). Green dots and dotted (green) lines represent the case of zero electric field, while red circles and solid (red) lines correspond to the electric field  $E = -1$  V/nm, and blue squares and dashed (blue) lines to the field  $E = 1$  V/nm. The magnetization orientation  $\theta$  is measured with respect to the  $[1\bar{1}0]$  crystallographic direction of GaAs.

respectively.

For illustration we show in Fig. 3 a comparison between the magnetization direction dependence of the  $n = 2$  band-energy gradient at the  $\Gamma$  point obtained from the *ab-initio* data and the corresponding fittings using Eqs.(20) and (21). The good agreement corroborates that the higher order terms in the series expansion can here be indeed neglected. The fittings are excellent even in the presence of a finite electrostatic field along the  $[001]$  axis, as can be appreciated from Fig. 3. This is because the presence of such an electrostatic field does not affect the symmetry considerations used in the derivation of Eqs. (18) and (19).

As discussed in the article the Bychkov-Rashba-type and Dresselhaus-type SOC parameters,  $\alpha_n$  and  $\beta_n$  respectively, can be introduced through the relations  $\eta_n^{(0)} = \beta_n - \alpha_n$  and  $\mu_n^{(0)} = \beta_n + \alpha_n$ . Therefore, according to Eq. (14), we obtain,

$$\alpha_n(\theta) = \sigma \left[ \frac{a_n(\theta) \cos \theta - b_n(\theta) \sin \theta}{\sin(2\theta)} \right] ; \quad \beta_n(\theta) = \sigma \left[ \frac{a_n(\theta) \cos \theta + b_n(\theta) \sin \theta}{\sin(2\theta)} \right], \quad (22)$$

which allow us to extract the dependence of  $\alpha_n(\theta)$  and  $\beta_n(\theta)$  on the magnetization orientation from the *ab-initio* data. By combining Eqs. (20), (21), and (22) we obtain the following expressions for the angular dependence of the Bychkov-Rashba-type and Dresselhaus-type SOC parameters,

$$\alpha_n(\theta) = \sigma \left[ A_n^{(+)} + B_n^{(+)} \cos(2\theta) + C_n^{(+)} \cos(4\theta) \right], \quad (23)$$

$$\beta_n(\theta) = \sigma \left[ A_n^{(-)} + B_n^{(-)} \cos(2\theta) + C_n^{(-)} \cos(4\theta) \right], \quad (24)$$

with  $A_n^{(\pm)}$ ,  $B_n^{(\pm)}$ , and  $C_n^{(\pm)}$  given by

$$A_n^{(\pm)} = \frac{a_{n0} + a_{n1} \pm (b_{n1} - b_{n0}) + a_{n2} \mp b_{n2}}{2}, \quad (25)$$

$$B_n^{(\pm)} = a_{n1} + a_{n2} \pm (b_{n2} - b_{n1}), \quad (26)$$

and

$$C_n^{(\pm)} = a_{n2} \mp b_{n2}, \quad (27)$$

respectively.

In the bottom panel of Fig. 3 of the article we show the magnetization direction dependence of the SOC parameters for the case of the interface band  $n = 2$  and three different values of the electrostatic field across the heterostructure. For the plots we used Eqs. (23)-(27) with the expansion coefficients  $a_{nl}$  and  $b_{nl}$  ( $l = 0, 1, 2$ ) obtained after the fitting in Fig. (3) and took into account that band  $n = 2$  exhibits spin-down character near the  $\Gamma$  point (i. e.  $\sigma = -1$ ).

<sup>1</sup> R. Winkler, H. Noh, E. Tutuc, and M. Shayegan, Phys. Rev. B **65**, 155303 (2002).

<sup>2</sup> R. Winkler, *Spin-orbit coupling effects in two-dimensional electron and hole systems* (Springer, Berlin, 2003).

<sup>3</sup> O. E. Raichev, Physica E **40**, 1662 (2008).

<sup>4</sup> A similar situation occurs in zinc-blende semiconductor quantum wells, where the quantum confinement splits the fourfold-degeneracy of the  $\Gamma_{8v}$  valence band into heavy-hole (HH) and light-hole (LH) subbands.<sup>1-3</sup> The splitting of the HH and LH subbands allows for a description of the SOC in terms of Pauli matrices.<sup>1-3</sup>

<sup>5</sup> Similarly, for  $\pi/2 \leq \theta < \pi$  a reflection with respect to the mirror plane (110) is equivalent to a rotation of the magnetization of the initial system by an angle  $\pi - 2\theta$  around the [001] axis. In such a case one obtains  $E_n(k_x, -k_y, \theta) = E_n(k_x, k_y, \pi - \theta)$ , which is the time reversal of the situation discussed in the text.

<sup>6</sup> A similar analysis for the case  $\pi/2 \leq \theta < \pi$  leads to the same expressions [Eqs. (10) and (11)] for the SOFs. Therefore, Eqs. (10) and (11) are valid for any value of  $\theta$ .